Sensors & Transducers, Vol. 171, Issue 5, May 2014, pp. 169-175

Sensors & Transducers

http://www.sensorsportal.com

A Piezoelectric Inchworm Actuator with Bidirectional Thrust Force

[1] Shunming HUA, [2] Guosong LIU, [1] Xiaojun WANG, [1] Yiqiang WANG and [1] Jialin LI

[1] Ningbo Institute of Technology, Zhejiang University,
No. 1, South Qianhu Road, Ningbo 315100, China
[2] Changchun Institute of Optics, Fine Mechanics and Physics, Chinese Academy of Sciences,
No. 3888, East Nanhu Avenue, Changchun 130033, China
[1] Tel.: +86-0574-88229521, fax: +86-0574-88229586
[1] E-mail: nithuasm@126.com

Received: 23 April 2014 /Accepted: 27 May 2014 /Published: 31 May 2014

Abstract: An inchworm actuator is designed as symmetrical structural layout, which can generate bidirectional thrust force. The clamped flexible mechanisms are set in stator and that of driven are in mover. Firstly, the parameters of flexible hinges are analyzed and optimized. Then, a kind of 6-division time-sequence signal applied to clamped/driven mechanism is discussed. As a result, trapezoid waveform is adopted which rise-rate is limited within 1 V/ms. Prototype actuator as well as specified three channels controller is finally manufactured and some tests are performed on them. The maximum step-length is 10.5 μm under 100 V. The displacement resolution is about 0.048 μm under 9 V. The maximum velocity and dynamic force are 412 μm/s and 2.85 Kgf separately. *Copyright © 2014 IFSA Publishing, S. L.*

Keywords: Piezoelectric actuator, Bidirectional thrust, Inchworm motion, Trapezoid time-sequence.

1. Introduction

Inchworm actuators have been widely used in precise positioning applications in recent decades, such as in situ tests, micromachining, autonomous robot, micromanipulation, and so on [1-5]. The step motion can be realized by inverse piezoelectric effects, piezohydraulic manners, electromagnetic effects, static electricity, ER effects, etc. [6-10]. The common method is piezoelectric stacks plus flexible hinge mechanisms. In general, traditional transmissions are relatively complex, lubrication need and occupy more space. But piezoelectric actuator has advantages of ultra-compact, high resolution, rapid response and low power consumption. In addition, the usage of flexible hinge makes seamless and frictionless transmission become possible. Therefore, the combination of them is the most suitable way to accomplish precise positioning.

For inchworm actuator, the preload force exerted between piezoelectric stack and flexible hinge is necessary and crucial. If the preload is excessive, the effective elongation of stack is deduced. The transmission efficiency is naturally lower than that of regular case. Conversely, if the preload is too small, the clearance between stack and hinge is incompletely diminished. Both transmitting precision and step stability are not satisfied. Most of traditional inchworm actuators output their bidirectional driving force/torque by stretching force from stack and

restoring force from hinge [11-13]. In order to make push and pull force in equilibrium, the preload exerted sometimes is up to half of nominal output force of stack. This excessive preload not only lowers transmission efficiency, but also generates extra heating and be harmful to service life of stack. A piezoelectric actuator with bidirectional thrust is put forward [14]. The motion backwards is not driven by restoring force, but by another stack. Although this design is a little complicated, the preload force can be adjusted to an appropriate value, especially suitable for applications where thrust requirement are not high.

2. Structural Design and Working Principle

Structural layout of the proposed prototype actuator illustrates in Fig. 1.

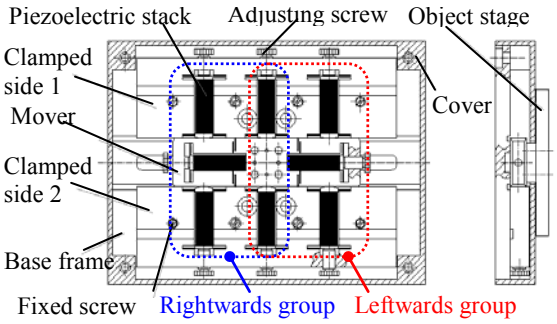

Fig. 1. Structure design and prototype photos of the actuator.

There are three pairs of symmetrical structural clamped stacks in the stator and there are 2 driving stacks in the mover.

Two left pairs of clamped stacks and the left driving stack constitute the rightwards group, which can achieve step motion rightwards. The right corresponding leftwards group can achieve step motion leftwards. Adjusting mechanism using optical fine screw to improve and adjust the resolution.

The actuator's working principle illustrates in Fig. 2. In the initial state, the middle pair of clamped stacks (name it as MCS later) is performed, in order to maintain the bearing capacity for the mover. Take leftwards motion for instance, the duty cycle is shown as follows. The left pair of clamped stacks (LCS) and the left driving stack (LDS) should be kept free all the time when the actuator is driven to move leftwards.

1) MCS are kept clamping and right pair of stacks (RCS) be clamped.
2) MCS are loosened.
3) Right driving stack (RDS) is elongated and the object stage is pushed leftwards in one step.
4) RCS are kept clamping and MCS are clamped again.
5) RCS are loosened.
6) RDS is reset and shortened. MCS should be kept clamping and prepared for the next duty cycle.

And similarly, the object stage can be driven rightwards by corresponding LDS and LCS. It is obviously that the actuator is driven by push force either moving leftwards or rightwards.

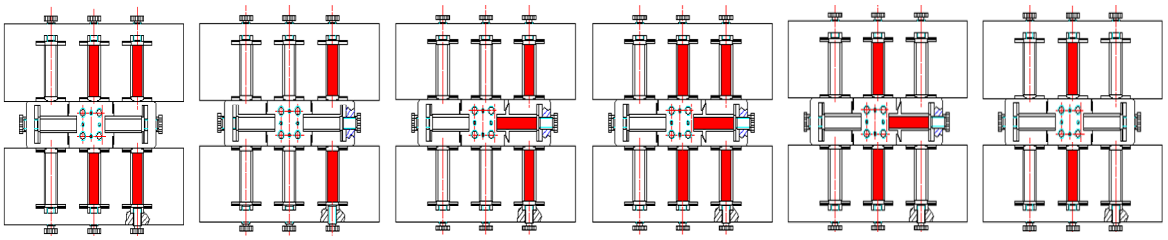

Fig. 2. Schematic diagram of the duty cycle.

3. Motion Characteristics Analysis

3.1. Frequency Response of Flexible Hinges

Inchworm motion includes six stages as described above, therefore, the clamped and driven mechanism must be operated coordinately, which are forced to vibrate by piezoelectric stacks. Actuator's working frequency depends on the lower one of the clamped and driven flexible hinges, because the piezoelectric stacks have high frequency response. The structural parameters of two flexible hinges are same in this paper as shown in Fig. 3. The following is mechanical analysis of the clamped mechanism for instance [15-16].

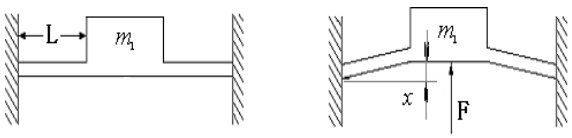

Fig. 3. Mechanical analysis to parallel flexible hinge.

Suppose the mass of clamped stack is m_1, the length of the cantilever and moment of inertia are L

and I separately, applied force is F, the displacement of the clamped stack is *x*, the average kinetic energy of the clamped stacks can be expressed as:

$$T_1 = m_1 \dot{x}^2 / 2, \quad (1)$$

Rotational kinetic energy of the flexible hinges is expressed as:

$$T_2 = 2 \cdot I \dot{\gamma}^2 / 2 = I \dot{\gamma}^2, \quad (2)$$

The total kinetic energy of the clamped system is expressed as:

$$T = T_1 + T_2 = m_1 \dot{x}^2 / 2 + I \dot{\gamma}^2, \quad (3)$$

where m_1 is the mass of the clamped stack; x is the displacement of the clamped stack; I is the moment of inertia the flexible hinge to endpoint, and $I=m_a L^2/3$, m_a is the mass of the flexible hinge; γ is the rotational angle of the cantilever.

Potential energy of the system is expressed as:

$$U = \frac{1}{2} K x^2, \quad (4)$$

where K is the rigidity of the flexible hinges.

Deformation energy of the flexible hinges is negligible because of stretching in the formula, by Lagrange equation:

$$\frac{d}{dt}\left(\frac{\partial T}{\partial \dot{q}}\right) - \frac{\partial T}{\partial q} = -\frac{\partial U}{\partial q}, \quad (5)$$

Take x as the generalized coordinates and we can obtain that:

$$\left(m_1 + \frac{2I}{L^2}\right)\ddot{x} + \frac{8K_z}{L^2} x = 0, \quad (6)$$

where $K \approx K_z / L^2$

The inherent frequency of the clamped system is expressed as:

$$\omega_n = \sqrt{\frac{8K_z}{m_1 L^2 + 2J}} = \frac{1}{L}\sqrt{\frac{24K_z}{3m_1 + 2m_a}}, \quad (7)$$

So

$$f = \omega_n / 2\pi = \frac{1}{2\pi L}\sqrt{\frac{24K_z}{3m_1 + 2m_a}}, \quad (8)$$

Then, the dimension parameters of clamped and driven hinges can be analyzed through ANSYS software based on expression (8). Finally, the optimized results of the parallel plate flexible hinge are as following. The length is 6 mm, the thickness is 0.5 mm, the width is 7 mm, the first-order inherent frequency is 150 Hz and the maximum output displacement is 11.4 μm.

3.2. Influence of Time-sequence Signals

Actuator motion characteristics are affected not only by natural frequency of the flexible hinges but also the time-sequence of the control signals. If two pairs of clamped mechanism unclamp at the same time during movement, the mover become freedom and lose driving ability instantaneously. In other words, the time-sequence signals should ensure two pairs of clamped mechanism have enough overlapping time, which can makes the mover is always locked during clamp alternation.

A time-sequence design which consists of six segmentations of duty cycle is proposed as shown in Fig. 4. Fig. 4(a) and Fig. 4(b) are rectangular and trapezoid waveform of time-sequence control separately.

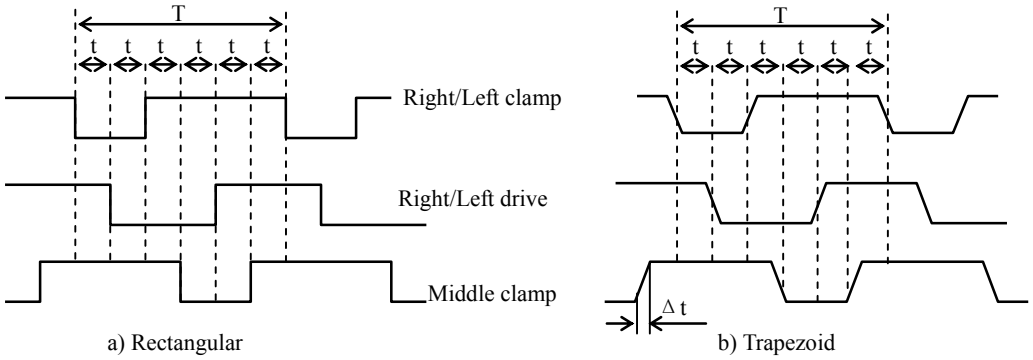

Fig. 4. Waveform of time sequence control.

A duty cycle is divided into six segmentations, the length of each part t=T/6. For clamped mechanism, low electrical level time 2t=T/3 and high level time 4t=2T/3.

For driven mechanism, high electrical level time is as the same as low level and occupies T/2 separately. The time-shift of two clamped signals is 3t.

The prototype actuator is initially controlled by rectangular waveform of time-sequence control, but the rise-rate of impulse is so fast that the clamped displacements overshoot and enhanced the impact to the mover. Finally, the waveform is improved by trapezoid waveform whose rise-rate of impulse is slow.

The piezoelectric stacks used in clamped and driven mechanisms are AE0505D16 manufactured by NEC of Japan. It is recommended that the nominated voltage is 100 V. The results of experiment show that when the rise-rate of trapezoid waveform is less than 1 V/ms, the clamped error (that means the displacement perturbation along movement direction generated by clamped impact) is far less than the displacement resolution. Regard this as the principle of waveform design, assume the rise time and fall time of trapezoid waveform is Δt separately, $\Delta t \approx t/4$.

Furthermore,

$$(U_H - U_L)/\Delta t \le 100V/ms, \quad (9)$$

where U_H is the clamped voltage 100 V; U_L is the zero voltage 0 V.

When Δt = 1 ms, the highest working frequency of trapezoid signal is 41.6 Hz. In order to maintain $\Delta t = 1ms$, the actual clamped and driving voltage will decrease when the frequency is higher than 41.6 Hz. The actual voltage can be calculated by equation (10).

$$U_{AH} = 1000U_S/(24f), \quad (10)$$

where U_{AH} is the actual clamped voltage (V); U_S is the working voltages setting 100 V; f is the frequency of trapezoid waveform.

That means the actual clamped as well as driven force will also decrease with voltage, therefore, actuator velocity will be lower.

4. Experimental Results and Discussion

Experimental system and prototype actuator illustrates in Fig. 5 and Fig. 6.

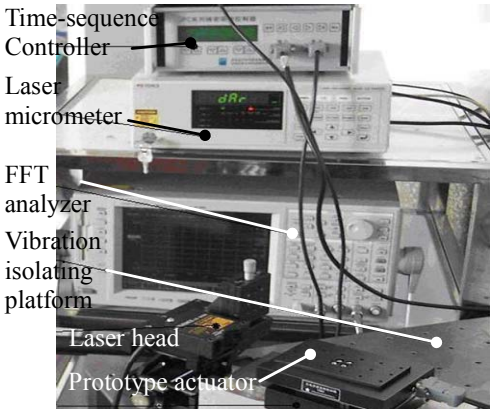

Fig. 5. Experimental system.

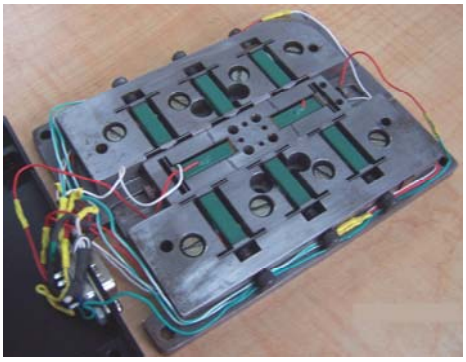

Fig. 6. Prototype actuator.

The prototype actuator is fixed on the vibration isolating platform and driven by specified 3-channel controller. The mover is taken non-contact measurement with the KEYENCE LC-2400A laser micrometer. The multi-function FFT analyzer CF5220 is used to analyze and process the signals. The measuring items include clamped characteristics, step-length as well as its stability, motion velocity and the driving force and so on.

4.1. Clamped Force

The clamped force is equal to the maximum static frictional force exerted on the mover by clamped stacks. Measuring method: Let the mover maintain its static position on condition that only one stack clamped, while use the fixed pulley, thin copper wire and tension meter to apply force. Laser micrometer displays the mover position and set its initial value as zero. Applied pulling force gradually till the laser micrometer displays the balanced state is destroyed, note down the force this moment as the clamped force under corresponding voltage.

In Fig. 7, there is no clamped force when clamped voltage is less than 40 V, it is because there is minimum fit clearance between the mover and clamped surface.

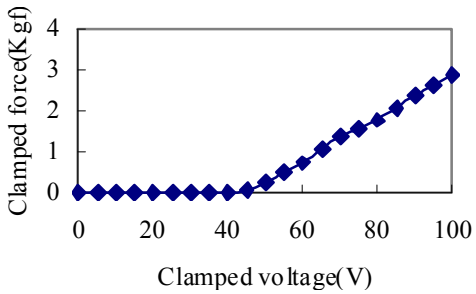

Fig. 7. Clamped force versus voltage.

Furthermore, the mover will give a little elastic deformation under clamped force because of its low rigidity. Then, the clamped force increase linearly while voltage is more than 40 V. The maximum

clamped force is 2.9 Kgf (about 28.4N) under 100 V. As well known, the maximum push force of AE0505D16 piezoelectric stack is about 850N theoretically under 100 V. If the friction coefficient is 0.1, the clamped force should be 85N. But the actual clamped force is only one third of the theoretical value. The reason is mover embedded driving stacks, and the rigidity is relatively small, partially counteract the clamped displacement.

4.2. Clamped Error

Clamped error means the displacement error along moving direction when two pairs of clamped stacks alternate run and driving stack don't work. It describes the influence of clamp motion on inchworm motion.

Let clamped stacks run alternately in 1min while driving stack don't run, then the maximum micro shift of mover is regarded as clamped error. Changing voltage from 0 to 100 V, obtain the clamped error results as shown in Fig. 8. The clamped error will be up to 0.12 μm when voltage is 100 V. It is obviously too large to precise motion. Therefore, when positioning accuracy requires high, the clamped voltage should be within 40 V and 75 V.

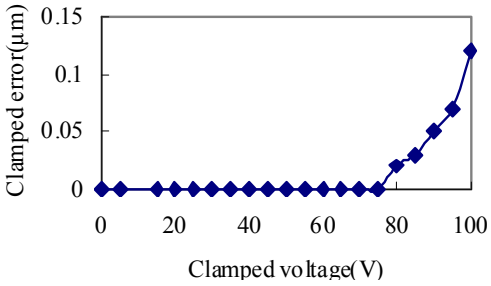

Fig. 8. Clamped error versus voltage.

Clamped error mainly comes from two aspects: one is mover's lateral deviation and deflection, the other is elastic deformation under clamped force. There are three corresponding ways to diminish error, increase assembly precision, reduce clamped voltage, increase rigidity of the mover.

4.3. Step-length and its Stability

Step-length of actuator is the stroke that mover runs in a duty cycle, and the shortest one is called displacement resolution under stable working condition. Step-length and displacement resolution are both important parameters to evaluate the performance of actuator.

Step-length of inchworm actuator is determined by displacement output of the driving stack under corresponding voltage. Meanwhile, it is also influenced by external force, just like frictional force, load, etc. The correlation curve between the no-load step-length and voltage is shown in Fig. 9, which has a good linearity.

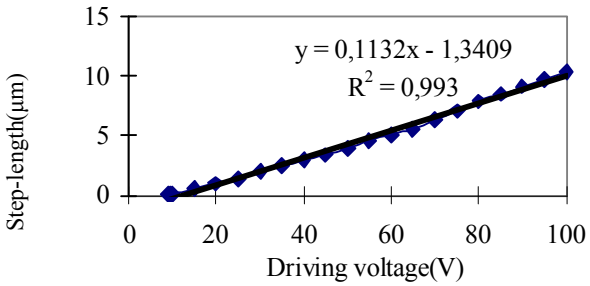

Fig. 9. Relationship between step-length and voltage under 1 Hz.

From Fig. 9, the maximum step-length of the actuator is 10.5 μm under no-load when the voltage is 100 V, and the shortest one is 0.048 μm under 9 V. The maximum step-length is approximately equal to the stack's nominal elongation which is 10.9 μm under 100 V.

But the shortest one is far less than the nominal elongation which is 0.64 μm under 9 V. The results show that frictional force has a great influence on moving performance when driving voltage is low. For this actuator, the nominal driving voltage should be more than 10 V.

Stability of step-length is another important index to evaluate movement precision. This paper use formula (11) to calculate and measure the step-length stability.

$$\eta_s = (\sum_{1}^{n} \left| \frac{S_i - \bar{S}_n}{\bar{S}_n} \right|) / n, \quad (11)$$

where η_s is the step-length stability of the actuator; S_i is the actual step-length; $\bar{S}_n$ is the average step-length after feed n steps; n is the number of feed steps.

The correlation curve between step-length stability and driving voltage is shown in Fig. 10.

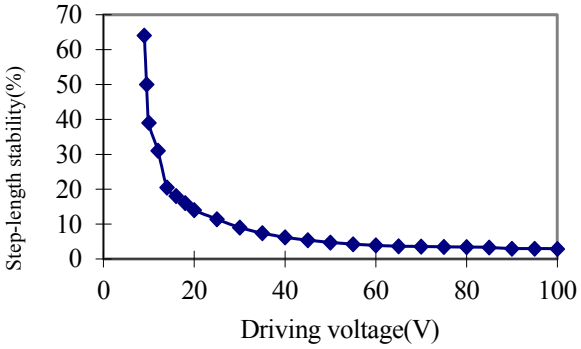

Fig. 10. Step-length stability versus driving voltage.

It is obviously that stability on 40 V is a critical point. On its right, the stability is satisfied. The stability decrease slowly with raising of voltage, and the best condition occurs on 100 V which is 2.9 %. On its left, the stability is very bad. The worst condition occurs on 9V and the value is up to 63%. The results show that the nominal voltage of the actuator should be higher than 40 V in consideration of step-length stability.

4.4. Velocity Analysis

In the condition of no-load, regard frequency as parametric variable, measure the correlation curve between velocity and voltage under different frequency. The results are as shown in Fig. 11. When the frequency is lower, the fluctuation of the curve is not obvious and the linearity is high. With increase of frequency, curve's fluctuation becomes obvious. This phenomenon shows, for the inchworm actuator, the stability under lower frequency is superior to that of higher.

Combining the analysis results in section 4.2, the ideal working conditions for the actuator with bidirectional thrust force are high voltage and low frequency, where stability of step-length and velocity are both satisfied. However, the clamped voltage should be low to decrease the clamped error.

The analyzing results in section 3.1 show that the first-order natural frequency of the flexible hinge is 150 Hz after optimization. But actually, if the working frequency is higher than 40 Hz, the motion velocity and driving force both fall rapidly. This is because the rise-rate of trapezoid waveform is limited in the specified 3-channel time-sequence controller. The experimental correlation curve between velocity and frequency is shown in Fig. 12. The maximum velocity of the actuator is 412 μm/s under 100 V and 40 Hz.

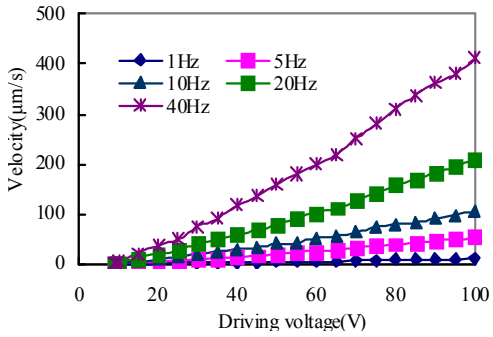

Fig. 11. Velocity versus voltage under different frequency.

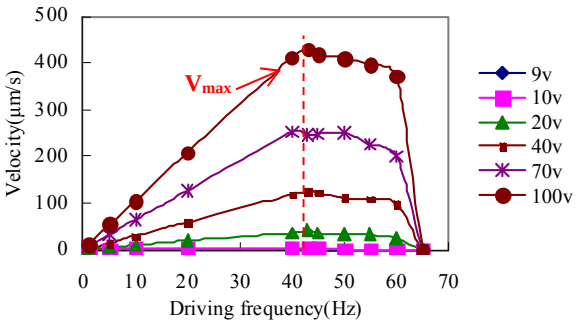

Fig. 12. Relationship between velocity and driving frequency.

4.5. Dynamic Driving Force

The output force of actuator is determined by thrust force from driving stacks and frictional force converted from clamped stacks. As this actuator adopts inner embedded driving mechanisms in order to output bidirectional thrust force, the rigidity of the mover are weakened partially, and the actual clamped force is smaller than the driving force. The maximum output force, therefore, is equal to the frictional force converted from the maximum clamped force.

The force when the mover realizes continuous inchworm motion with load is called dynamic driving force or continuous driving force. Measurement method: hang some weights on the mover through a fixed pulley and thin copper wires, use laser micrometer to record inchworm motion of the mover. Set driving frequency on fixed 10 Hz, clamped voltage 100 V, and driving voltage from 10 V to 100 V. Under some driving voltage, increase weight gradually till the mover occur out-of-step. The weight at this time is regarded as the maximum dynamic driving force under this voltage. The correlation curve between the maximum dynamic driving force and driving voltage is shown in Fig. 13.

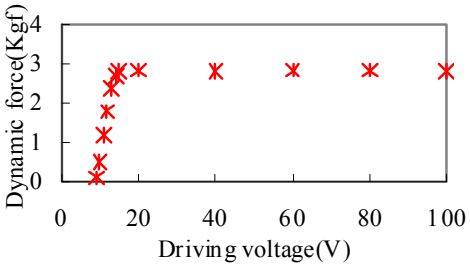

Fig. 13. Dynamic force versus driving voltage.

The maximum dynamic driving force increase rapidly under driving voltage between 10 V and 14 V, the force is up to about 2.7 Kgf under 14 V. And then, the dynamic force maintains about 2.85 Kgf, slightly smaller than the maximum clamped force 2.9 Kgf, that is because the actuator affected by frictional force and fluctuation of clamped force during alternation.

5. Conclusions

The inchworm actuator realizes bidirectional thrust operation mode through symmetrical design.

One cycle of time-sequence signal is divided into 6 stages to match driven & clamped signals. For waveform, trapezoid is superior to rectangular. In particular, the rise-rate of impulse should be limited within 1V/ms to decrease clamped shock and error.

Prototype actuator and specified 3-channel controller are manufactured. Some performances are tested on them and main results are as follows. The nominal driving voltage should be greater than 40 V considering step stability. And clamped voltage should be within 40~75 V in view of decrease clamped error. The maximum step-length and velocity are 10.5 μm and 412 μm/s under 100 V. The displacement resolution is about 0.048 μm under 9 V. The maximum dynamic force is about 2.85 Kgf.

Experimental results prove the inchworm actuator can meet the need of precise positioning. And next, improving stiffness of mover is the key factor to increase precision and force.

Acknowledgements

This research is supported by the National Natural Science Foundation of China (Grant Nos. 51275467). The authors wish to thank Professors Guangming Cheng, Zhigang Yang and Ping Zeng from Jilin University for their valuable suggestions and contribution to this work.

References

[1]. Z. C. Ma, H. W. Zhao, Q. C. Li et al., Novel in situ device for investigating the tensile and fatigue behaviors of bulk materials, *Review of Scientific Instruments*, Vol. 84, Issue 4, 2013, pp. 1-9.

[2]. S. T. Lee, K. L. Huang, J. W. Wu et al., Design and control of long travel range electromagnetically actuated positioning stage with application to precise machining, in *Proceedings of the IEEE International Conference on Control Applications,* Yokohama, Japan, 8-10 September 2010, pp. 2219-2224.

[3]. H. Ikeda, T. Morita, High-precision positioning using a self-sensing piezoelectric actuator control with a differential detection method, *Sensors and Actuators A: Physical,* Vol. 170, Issue 1-2, 2011, pp. 147-155.

[4]. Y. Tian, B. Shirinzadeh, Design and dynamics of a 3-DOF flexure-based parallel mechanism for micro/nano manipulation, *Microelectronic Engineering*, Vol. 87, Issue 2, 2010, pp. 230–241.

[5]. H. Zhou, Y. M. Pei, H. Huang et al., Multi-field nanoindentation apparatus for measuring local mechanical properties of materials in external magnetic and electric fields, *Review of Scientific Instrument*, Vol. 84, Issue 6, 2013, pp. 1-6.

[6]. R. J. E. Merry, N. C. T. de Kleijn, M. J. G. van de Molengraft et al., Using a walking piezo actuator to drive and control a high-precision stage, *IEEE/ASME Transactions on Mechatronics*, Vol. 14, Issue 1, 2009, pp. 21-31.

[7]. J. W. Kan, S. Y. Wang, Z. H. Zhang et al., Development of piezohydraulic actuator driven by piezomembrane pump, *Journal of Intelligent Material Systems and Structures,* Vol. 22, Issue 16, 2011, pp. 1829-1840

[8]. Y. C. Liang, M. Taya, J. Q. Xiao et al., Design of an inchworm actuator based on a ferromagnetic shape memory alloy composite, *Smart Materials and Structures*, Vol. 21, Issue 11, 2012, pp. 1-8.

[9]. M. A. Erismis, H. P. Neves, R. Puris et al., Saw-tooth vernier ratchets for electrostatic inchworm actuators, *Sensors and Actuators A: Physical,* Vol. 156, Issue 1, 2009, pp. 66-71.

[10]. C. H. Li, Y. G. Meng, Y. Tian, Recession in a linear stepper motor based on piezoelectric actuator and electrorheological clampers, *Smart Materials and Structures*, Vol. 21, Issue 12, 2012, pp. 1-8.

[11]. H. W. Zhao, L. Fu, L. Q. Ren et al., Design and experimental research of a novel inchworm type piezo-driven rotary actuator with the changeable clamping radius, *Review of Scientific Instruments*, Vol. 84, Issue 1, 2013, pp. 1-9.

[12]. C. H. Oh, J. H. Choi, H. J. Nam et al., Ultra-compact, zero-power magnetic latching piezoelectric inchworm motor with integrated position sensor, *Sensors and Actuators A: Physical*, Vol. 158, Issue 2, 2010, pp. 306-312.

[13]. O. Fuchiwaki, K. Alafuka, S. Omura, Development of 3-DOF inchworm mechanism for flexible, compact, low-Inertia, and omnidirectional precise positioning-dynamical analysis and improvement of the maximum velocity, *IEEE/ASME Transactions on Mechatronics,* Vol. 17, Issue 4, 2012, pp. 697-708.

[14]. W. S. Wang, S. T. Lucic, W. L. Brown et al., Design of a bidirectional MEMS actuator with high displacement resolution, large driving force and power-free latching, *Microelectronic Engineering*, Vol. 85, Issue 3, 2008, pp. 587-598.

[15]. H. Huang, H. W. Zhao, Z. C. Ma et al., Design and analysis of the precision-driven unit for nano-indentation and scratch test, *Journal of Manufacturing Systems*, Vol. 31, Issue 1, 2012, pp. 76-81

[16]. B. Song, Y. Yu, W. C. Yang et al., Research of micro/nano displacement sensor for piezoelectric actuator, in *Proceedings of the International Conference on Robotics and Biomimetics*, Bangkok, Thailand, 21-26 February 2008, pp. 269-275.

[17]. J. P. Li, H. W. Zhao, H. Qu et al., A piezoelectric-driven rotary actuator by means of inchworm motion, *Sensors and Actuators A: Physical*, Vol. 194, 2013, pp. 269-276.

[18]. Q. S. Xu, Y. M. Li, Dahl model-based hysteresis compensation and precise positioning control of an XY parallel micromanipulator with piezoelectric actuation, *Journal of Dynamic Systems, Measurement, and Control*, Vol. 132, Issue 4, 2010, pp. 1-12.